Viscosity of Dilute Suspensions of Rigid Bead Arrays at Low Shear: Accounting for the Variation in Hydrodynamic Stress Over the Bead Surfaces

Stuart A. Allison* and Hongxia Pei

Department of Chemistry, Georgia State University, Atlanta, Georgia 30302-4098

Received: January 6, 2009; Revised Manuscript Received: April 22, 2009

In this work, we examine the viscosity of a dilute suspension of irregularly shaped particles at low shear. A particle is modeled as a rigid array of nonoverlapping beads of variable size and geometry. Starting from a boundary element formalism, approximate account is taken of the variation in hydrodynamic stress over the surface of the individual beads. For a touching dimer of two identical beads, the predicted viscosity is lower than the exact value by 5.2%. The methodology is then applied to several other model systems including tetramers of variable conformation and linear strings of touching beads. An analysis is also carried out of the viscosity and translational diffusion of several dilute amino acids and diglycine in water. It is concluded that continuum hydrodynamic modeling with stick boundary conditions is unable to account for the experimental viscosity and diffusion data simultaneously. A model intermediate between "stick" and "slip" could possibly reconcile theory and experiment.

I. Introduction

Measurement of the incremental change of the viscosity of a dilute suspension with solute concentration provides a simple and inexpensive way of obtaining information about macromolecular size and shape in solution.[1,2] Theoretical modeling was initially limited to simple geometries such as solid spheres[3] and axisymmetric ellipsoids.[4] In the 1940s, viscosity theory was extended to flexible polymers modeled as random coils[5] and porous spheres.[6] Later investigators refined and generalized the "bead method" of Kirkwood and Riseman[5] and modeled macromolecules as rigid arrays of beads.[7−11] A methodology that is very closely related to the "bead method" is the boundary element (BE) method in which the macromolecular surface is represented as a closed surface of interconnected plates.[12−15] In this latter method, the problem can be formulated as an integral equation. In the limit of many plates, the BE approach has been shown to be exact for certain model geometries.[15,16] It is fair to say that, for model particles of arbitrary size, it is possible to accurately determine the corresponding intrinsic viscosity, or viscosity shape factor, subject to the limitations of continuum fluid mechanics and the corresponding hydrodynamic boundary conditions at the particle/fluid interface.

A disadvantage of both bead and BE methodologies is the necessity of using large numbers of beads or plates in modeling a particular structure. For proteins modeled as bead arrays, bead overlap has been a problem that has been difficult to deal with when the overlapping beads are of unequal size.[9,10,17−19] Although approximate hydrodynamic interaction tensors have been developed[17,18] and systematically tested[19] to deal with this problem, the current strategy in most widespread use is to use large numbers of nonoverlapping beads that closely conform to the topography of the structure being modeled.[10,20,21] (See Figure 1.) For large N, where N is the number of beads [10,21] or plates [14−16] used, a smooth surface representing the solvent−particle interface is more readily modeled by a series of interconnected plates (BE approach) than as a bead array and the "overlap" problem does not arise. However, regardless of whether the bead or BE approach is used, computation time varies as N^3, which limits the investigator to several thousand beads or plates.[10,14−16,21] Many beads or plates are used for two reasons: the first reason is that this approach yields a more accurate surface model. The second reason is related to the fact that hydrodynamic stresses vary continuously over the surface of the particle. However, in both bead and BE modeling, it is usually assumed that the hydrodynamic stresses are uniform over the individual surface elements, but can vary between neighbors. Also, the accuracy of the "constant stress" assumption depends not only on the relative bead or plate size, but also on the transport phenomena being studied. For example, the approximation is more accurate in modeling translational friction than rotational friction or viscosity. It was recognized some time ago that, for model structures made up of few beads and for the transport properties of rotational friction and viscosity, failure to account for stress variations over individual beads led to substantial error.[22−24] By increasing the number of beads or plates and reducing their size relative

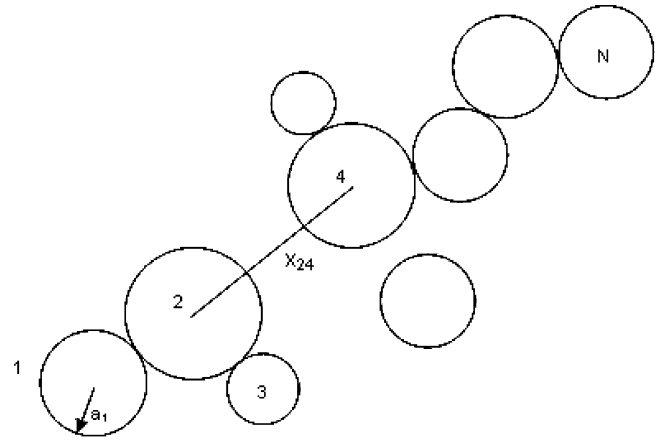

Figure 1. Schematic of the general bead model. The model is represented as N beads of variable radius a_j. The arrangement of the beads is arbitrary. The beads may touch, but cannot overlap.

* Corresponding author. E-mail: sallison@gsu.edu.

10.1021/jp9001109 CCC: $40.75
Published on Web 05/19/2009

to the particle being modeled, the assumption of constant stress over the individual surface elements becomes progressively better. The "shell model" (covering the surface with a large number of nonoverlapping beads) was originally proposed by Bloomfield and Filson[22] and remains in widespread use to the present day.[20,21] This approach does, however, cost more from the standpoint of computation time and simply becomes prohibitive for model structures made up of more than several thousand beads or plates. Fortunately, the extrapolation to an infinite number of plates of vanishing size is straightforward. One promising alternative involves extended Kirkwood−Riseman or "multipolar" treatments, in which higher order terms with regard to a/r (a is a bead radius and r is an interbead distance) are included in the intersubunit hydrodynamic interaction tensors of multibead arrays.[21,25−29] The "multipolar" approaches have been used extensively in treating the relative motion of bead arrays including concentrated suspensions.[28,29] In an application that is relevant to the present work, Fixman has applied a "multipolar" approach to account for the possible vanishing or negative intrinsic viscosity of a suspension.[27]

Another alternative starts from the BE formalism and an integral equation for the hydrodynamic stress on a model particle. This approach was applied to the translational friction of a bead array in an effective medium.[30] Following this systematic and straightforward procedure, it is possible, at varying levels of approximation, to account for the variation in stresses over individual beads. In the present work, this approach shall be extended to the problem of the viscosity of a dilute suspension of bead arrays. By doing so, we shall show that it is possible to obtain intrinsic viscosities, or viscosity shape factors, that are accurate to within several percent of exact values and using comparatively few beads in modeling the actual structure.

The outline of this paper is as follows. The methodology is formulated in section II and this section is divided into three subsections: II.A, II.B, and II.C. In subsection II.A, the underlying model is presented and developed for a bead array in a shear field within the BE formalism. This approach leads, in a systematic way, into the variation in stresses over individual beads in subsection II.B. In subsection II.C, the formal methodology for determining the viscosity shape factors and how they can be related to experiment are presented. In section III, the methodology is applied to three separate problems. The accuracy of the methodology is examined in subsection III.A by examining a dumbbell dimer of two identical beads. In subsection III.B, we compare viscosities of "straight rod" bead and cylinder models and also examine the sensitivity of viscosity and bead conformation for several tetramer bead models. In subsection III.C, we apply our methodology to modeling the viscosity of dilute aqueous solutions of several amino acids and also diglycine where experimental data are available. These are small molecules comparable in size to the solvent molecules themselves and, as such, provide a severe test of continuum hydrodynamic modeling when the "solute" particles are small. When the combined transport studies of translational diffusion and dilute solution viscosity are examined, we conclude that continuum hydrodynamic modeling employing "stick" boundary conditions cannot account for experiment in these systems. We conclude with a brief summary of the principal findings of this paper in section IV and give directions for possible future study.

II. Theory/Methodology

II.A. Velocity Field of a Bead Array Placed in a Shear Field. The fluid is assumed to obey the low Reynolds number Navier−Stokes and solvent incompressibility equations[31,32]

$$\eta_0 \nabla^2 \mathbf{v}(\mathbf{x}) - \nabla p(\mathbf{x}) = -\mathbf{s}(\mathbf{x}) \tag{1}$$

$$\nabla \cdot \mathbf{v}(\mathbf{x}) = 0 \tag{2}$$

where η_0 is the solvent viscosity, $\mathbf{v}(\mathbf{x})$ is the local fluid velocity at point $\mathbf{x}$ in the fluid, $p(\mathbf{x})$ is the local pressure, and $\mathbf{s}(\mathbf{x})$ is the local external force/unit volume on the fluid. For weakly charged bead arrays, where the primary electroviscous effect is small, a good approximation is to set $\mathbf{s}(\mathbf{x}) = \mathbf{0}$ in eq 1.[33−36] For now, however, we shall retain $\mathbf{s}(\mathbf{x})$. The hydrodynamic stress tensor is defined by

$$\sigma(\mathbf{x}) = -p(\mathbf{x})\boldsymbol{I} + \eta_0(\nabla v(\mathbf{x}) + \nabla v(\mathbf{x})^{\mathrm{T}}) \tag{3}$$

where $\mathbf{I}$ is the 3×3 identity tensor and superscript "T" denotes the transpose.[32,33] It is readily verified that $\boldsymbol{\sigma}$ is a symmetric tensor.

In the absence of our bead array, it shall be assumed that the local fluid velocity, $\mathbf{v}$, or ambient fluid velocity at point $\mathbf{x}$, $\mathbf{v}^0(\mathbf{x})$, can be written

$$\mathbf{v}^0(\mathbf{x}) = \mathbf{u}^0 + \frac{1}{2}\boldsymbol{A} \cdot (\mathbf{x} - \mathbf{d}) \tag{4}$$

where $\mathbf{u}^0$ and $\mathbf{d}$ are constant vectors and $\mathbf{A}$ is a traceless second rank tensor. Also, $p^0(\mathbf{x}) = 0$. We can identify $\mathbf{u}^0$ with the drift velocity of the fluid in some convenient laboratory frame of reference. The requirement that $\mathbf{A}$ is traceless is necessary to ensure that $\mathbf{v}(\mathbf{x})$ obeys eq 2. It is convenient to write $\mathbf{A}$ as

$$\boldsymbol{A} = \boldsymbol{W} + \boldsymbol{E} \tag{5}$$

where $\mathbf{W}$ is an antisymmetric tensor and $\mathbf{E}$ is a symmetric tensor. $\mathbf{W}$ represents the local rotation of the fluid about $\mathbf{x} = \mathbf{d}$, and $\mathbf{E}$ represents the deformational shear of the fluid. From eq 3, the hydrodynamic stress of our ambient fluid flow is

$$\sigma^0 = \eta_0 \boldsymbol{E} \tag{6}$$

Into this ambient fluid, our bead array is now placed. Under steady state conditions, it translates with velocity $\mathbf{u}_0$ and rotates with angular velocity $\boldsymbol{\omega}$ about point $\mathbf{x} = \mathbf{d}$ in the fluid. In general, the center of rotation can be determined for arbitrary model bead arrays using established procedures.[8] In practice, the center of rotation can be equated to the center of mass (assuming beads are comprised of material of the same density for all beads) to a good approximation. This is done in the present work.

Stick hydrodynamic boundary conditions are assumed to prevail at the fluid−particle interface. At a point on the surface of bead K, $\mathbf{y}_k$, the fluid velocity matches the rigid body motion (rbm), of the bead array

$$\mathbf{v}(\mathbf{y}_k) = \mathbf{u}^0 + \frac{1}{2}\boldsymbol{W} \cdot (\mathbf{y}_k - \mathbf{d}) = \mathbf{u}^0 + \omega \wedge (\mathbf{y}_k - \mathbf{d}) \tag{7}$$

In the second equality on the right-hand side of eq 7, "$\wedge$" denotes the vector cross product; $\mathbf{W}$ and $\boldsymbol{\omega}$ are related by

$$W_{ij} = -2\sum_k \epsilon_{ijk}\omega_k \tag{8}$$

where ϵ_{ijk} is the Levita-Civita symbol (ϵ_{ijk} vanishes if any of the three indices are equal; it equals 1 for even permutations of indices ((i,j,k) = (1,2,3), (3,1,2), (2,3,1)), and equals −1 for odd permutations ((i,j,k) = (1,3,2), (3,2,1), (2,1,3))).

Next consider the singular solution of eqs 1 and 2:

$$\eta_0\nabla^2\mathbf{v}^i(\mathbf{x},\mathbf{y}) - \nabla p^i(\mathbf{x}) = -\mathbf{e}_i\delta(\mathbf{x}-\mathbf{y}) = -\mathbf{s}^i(\mathbf{x}) \tag{9}$$

In eq 9, δ represents the delta function and $\mathbf{e}_i$ is a unit vector in direction i. Also define $\mathbf{r} = \mathbf{x} - \mathbf{y}$; the singular velocity and pressure are given by[32]

$$\mathbf{v}^i(\mathbf{x},\mathbf{y}) = \frac{1}{8\pi\eta r}\left(\boldsymbol{I} + \frac{1}{r^2}\boldsymbol{rr}\right)\cdot\mathbf{e}_i = \boldsymbol{U}(\mathbf{r})\cdot\mathbf{e}_i \tag{10}$$

$$p^i(\mathbf{x}) = \frac{1}{4\pi\eta r^3}\mathbf{r}\cdot\mathbf{e}_i = \mathbf{P}(\mathbf{r})\cdot\mathbf{e}_i \tag{11}$$

The corresponding stress tensor for this singular solution is[32]

$$(\sigma^i(\mathbf{x},\mathbf{y}))_{jk} = -\frac{3}{4\pi r^5}r_i r_j r_k \tag{12}$$

This singular solution plays a vital role in both bead and the more general boundary element methodologies. Consider next the differential form of the Lorentz reciprocal theorem applied to a general field ($\mathbf{v}$, $\mathbf{s}$, $\boldsymbol{\sigma}$) and the singular field ($\mathbf{v}^i$, $\mathbf{s}^i$, $\boldsymbol{\sigma}^i$):[32]

$$\mathbf{s}^i\cdot\mathbf{v} + \nabla\cdot(\mathbf{v}\cdot\sigma^i) = \mathbf{s}\cdot\mathbf{v}^i + \nabla\cdot(\mathbf{v}^i\cdot\sigma) \tag{13}$$

Consider first the actual fluid velocity of our bead array and take the domain of integration, V_e, to be the fluid outside of the volume occupied by the individual beads, but within a large sphere of radius b ($b \gg L$, where L is the largest physical dimension of our bead array.) Integrate eq 13 over this domain and use the divergence theorem on the "∇" terms.

$$v_i(\mathbf{y})\,\Phi(\mathbf{y},V_e) + \int_{S_b}\mathbf{v}(\mathbf{x})\cdot\sigma^i(\mathbf{r})\cdot\mathbf{n}(\mathbf{x})\,dS_x - \sum_{J=1}^{N}\int_{S_J}\mathbf{v}(\mathbf{x})\cdot\sigma^i(\mathbf{r})\cdot\mathbf{n}(\mathbf{x})\,dS_x = \int_{S_b}\mathbf{v}^i(\mathbf{r})\cdot\sigma^i(\mathbf{x})\cdot\mathbf{n}(\mathbf{x})\,dS_x - \sum_{J=1}^{N}\int_{S_J}\mathbf{v}^i(\mathbf{r})\cdot\sigma^i(\mathbf{x})\cdot\mathbf{n}(\mathbf{x})\,dS_x + \int_{V_e}\mathbf{v}^i(\mathbf{r})\cdot\mathbf{s}(\mathbf{x})\,dV_x \tag{14}$$

In eq 14, S_b denotes the outer surface, S_J is the surface of bead J, and $\mathbf{n}(\mathbf{x})$ is the local outward unit normal to the respective surface. Also, $\Phi(\mathbf{y},V_e)$ equals 1 if $\mathbf{y}$ lies within V_e, it equals 0 if $\mathbf{y}$ lies outside V_e, and it equals 1/2 if $\mathbf{y}$ lies on the boundary surface.

The surface integrals at S_b can be eliminated as follows. Consider the flow field in the absence of the bead array defined by eqs 4−6; use this in eq 13, but take the domain of integration to be everything within the sphere of radius b, V_b.

In this case, eq 14 is replaced with

$$v_i^0(\mathbf{y})\,\Phi(\mathbf{y},V_b) + \int_{S_b}\mathbf{v}^0(\mathbf{x})\cdot\sigma^i(\mathbf{r})\cdot\mathbf{n}(\mathbf{x})\,dS_x = \int_{S_b}\mathbf{v}^i(\mathbf{r})\cdot\sigma^0(\mathbf{x})\cdot\mathbf{n}(\mathbf{x})\,dS_x \tag{15}$$

Far from the bead array ($|\mathbf{x}| \approx b$)

$$\mathbf{v}(\mathbf{x}) \approx \mathbf{v}^0(\mathbf{x}) + \delta\mathbf{v}(\mathbf{x}) \tag{16}$$

$$\sigma(\mathbf{x}) \approx \sigma^0(\mathbf{x}) + \delta\sigma(\mathbf{x}) \tag{17}$$

where the disturbance times (second terms on the right-hand sides of eqs 16 and 17 make no contribution to the surface integrals over S_b. Thus, we can use eq 15 to eliminate these

$$v_i(\mathbf{y})\,\Phi(\mathbf{y},V_e) - \sum_{J=1}^{N}\int_{S_J}\mathbf{v}(\mathbf{x})\cdot\sigma^i(\mathbf{r})\cdot\mathbf{n}(\mathbf{x})\,dS_x = v_i^0(\mathbf{y})\,\Phi(\mathbf{y},V_b) - \sum_{J=1}^{N}\int_{S_J}\mathbf{v}^i(\mathbf{r})\cdot\sigma(\mathbf{x})\cdot\mathbf{n}(\mathbf{x})\,dS_x + \int_{V_e}\mathbf{v}^i(\mathbf{r})\cdot\mathbf{s}(\mathbf{x})\,dV_x \tag{18}$$

The surface terms appearing on the left-hand side of eq 18 can also be eliminated. On S_J, the fluid obeys rbm similar to that defined by eq 7. Consider the flow field $\mathbf{v}(\mathbf{x}) = \mathbf{u}_0 + (1/2)\mathbf{W}\cdot(\mathbf{x}-\mathbf{d})$, $\mathbf{s}(\mathbf{x}) = p(\mathbf{x}) = 0$. For this field, we also know $\boldsymbol{\sigma}(\mathbf{x}) = 0$. Use this field in eq 13 and take the domain of integration to be the volume occupied by bead J.

$$[u_i^0 + \frac{1}{2}\sum_j W_{ij}(y_j - d_j)]\,\Phi(\mathbf{y},V_J) = -\int_{S_J}\mathbf{v}(\mathbf{x})\cdot\sigma^i(\mathbf{r})\cdot\mathbf{n}(\mathbf{x})\,dS_x \tag{19}$$

Use this in eq 18:

$$v_i(\mathbf{y})\,\Phi(\mathbf{y},V_e) + \sum_{J=1}^{N}[u_i^0 + \frac{1}{2}\sum_j W_{ij}(y_j - d_j)]\,\Phi(\mathbf{y},V_J) = v_i^0(\mathbf{y})\,\Phi(\mathbf{y},V_b) + \sum_{J=1}^{N}\int_{S_J}\mathbf{v}^i(\mathbf{r})\cdot\mathbf{f}(\mathbf{x})\,dS_x + \int_{V_e}\mathbf{v}^i(\mathbf{r})\cdot\mathbf{s}(\mathbf{x})\,dV_x \tag{20}$$

In eq 20, $\mathbf{f}(\mathbf{x})$ is the hydrodynamic force/area exerted by the respective bead on the surrounding fluid

$$\mathbf{f}(\mathbf{x}) = -\sigma(\mathbf{x})\cdot\mathbf{n}(\mathbf{x}) \tag{21}$$

For a point, $\mathbf{y}$, in the fluid (and within V_b)

$$v_i(\mathbf{y}) = v_i^0(\mathbf{y}) + \sum_{J=1}^{N}\int_{S_J}\mathbf{v}^i(\mathbf{r})\cdot\mathbf{f}(\mathbf{x})\,dS_x + \int_{V_e}\mathbf{v}^i(\mathbf{r})\cdot\mathbf{s}(\mathbf{x})\,dV_x \tag{22}$$

For a point at the center of bead K, $\mathbf{y} = \mathbf{x}_K$, eq 20 reduces to

$$-\frac{1}{2}\boldsymbol{E}\cdot(\mathbf{x}_K - \mathbf{d}) = \sum_{J=1}^{N} \int_{S_J} \boldsymbol{U}(\mathbf{x} - \mathbf{x}_K)\cdot\mathbf{f}(\mathbf{x})\, \mathrm{d}S_x + \int_{V_e} \boldsymbol{U}(\mathbf{x} - \mathbf{x}_K)\cdot\mathbf{s}(\mathbf{x})\, \mathrm{d}V_x \quad (23)$$

In eq 23, **U** is the symmetric (Oseen) tensor defined by the right-hand side of eq 10. It should be emphasized that "stick" hydrodynamic boundary conditions are assumed to prevail at the fluid−bead interface. We now must examine how $\mathbf{f}(\mathbf{x})$ varies over the surface of an individual bead. It shall be convenient to write $\mathbf{f}(\mathbf{x})$ (on bead J)

$$\mathbf{f}(\mathbf{x}) = \frac{1}{S_J}\mathbf{F}_J + \mathbf{g}(\mathbf{x}) \quad (24)$$

where S_J is the surface area of bead J and $\mathbf{F}_J$ is the net force exerted by bead J on the surrounding fluid. All of the variation of $\mathbf{f}$ over the bead surface is contained in $\mathbf{g}(\mathbf{x})$.

II.B. Variation in f(x) over a Particular Bead. From eq 1, we have $\nabla p = \eta_0\nabla^2\mathbf{v} + \mathbf{s}$ and can compute ∇p in the fluid from eq 22. Following this by subsequent integration, we can write for a point, $\mathbf{y}$, in the fluid.

$$p(\mathbf{y}) = p^0(\mathbf{y}) - \sum_{J=1}^{N} \int_{S_J} \mathbf{P}(\mathbf{r})\cdot\mathbf{f}(\mathbf{x})\, \mathrm{d}S_x - \int_{V_e} \mathbf{P}(\mathbf{r})\cdot\mathbf{s}(\mathbf{x})\, \mathrm{d}V_x \quad (25)$$

From eqs 3, 22, and 25, the stress at point $\mathbf{y}$ in the fluid can be written

$$\sigma_{ij}(\mathbf{y}) = \sigma^0_{ij}(\mathbf{y}) - \sum_{J=1}^{N}\sum_{k=1}^{3} \int_{S_J} \sigma^k_{ij}(\mathbf{r})\, f_k(\mathbf{x})\, \mathrm{d}S_x - \sum_{k=1}^{3} \int_{V_e} \sigma^k_{ij}(\mathbf{r})\, s_k(\mathbf{x})\, \mathrm{d}V_x \quad (26)$$

It should be emphasized that $\sigma^0_{ij}(\mathbf{y})$ is the local fluid stress in the absence of a bead array. Choose $\mathbf{y}$ to be a point in the fluid domain but near the surface of bead K; this point shall be denoted $\mathbf{y}_K{}^+$ where the "+" superscript emphasizes that the point is in the fluid domain and not on S_K. The latter point on S_K shall be designated $\mathbf{y}_K$. It is important to make this distinction due to the singular nature of some of the integrals involved. Next multiply eq 26 by $-n_j(\mathbf{y}_K)$ and sum over j. For the applications of interest in the present work, it shall be assumed that $\mathbf{s} = 0$ from here on. From eq 21

$$f_i(\mathbf{y}_K) = f_i^0(\mathbf{y}_K) + \sum_{j,k=1}^{3} n_j(\mathbf{y}_K) \int_{S_K} \sigma^k_{ij}(\mathbf{r}_K{}^+)\, f_k(\mathbf{x})\, \mathrm{d}S_x + \sum_{J\neq K}^{N}\sum_{j,k=1}^{3} n_j(\mathbf{y}_K) \int_{S_J} \sigma^k_{ij}(\mathbf{r}_K)\, f_k(\mathbf{x})\, \mathrm{d}S_x \quad (27)$$

In eq 27, $\mathbf{r}_K{}^+ = \mathbf{x} - \mathbf{y}_K{}^+$ and $\mathbf{r}_K = \mathbf{x} - \mathbf{y}_K$. For the surface integrals over $J \neq K$, we can replace $\mathbf{y}_K{}^+$ with $\mathbf{y}_K$ since the integrals are nonsingular.

The velocity and pressure field of a single sphere in a shear field are given on page 77 of ref 37. From these, it can be shown

$${}^{(0)}\mathbf{f}(\mathbf{y}_K) = {}^{(0)}\mathbf{g}(\mathbf{y}_K) = -\frac{5}{2}\eta_0\boldsymbol{E}\cdot\mathbf{n}(\mathbf{y}_K) \quad (28)$$

The "(0)" superscript above emphasizes that this is for a single isolated sphere in a shear field. In this case, there is no net force on the sphere (${}^{(0)}\mathbf{F}_K = 0$). Equation 24 is next used in eq 27. For the $\mathbf{g}$ terms appearing on the right-hand side of eq 27, we approximate them with eq 28. The net forces, $\mathbf{F}_K$ and $\mathbf{F}_J$, are retained. It can be shown that eq 27 reduces to

$$g_i(\mathbf{y}_K) \approx -\frac{5}{2}\eta_0\sum_j E_{ij}n_j(\mathbf{y}_K) + \sum_{jk}\sum_{J\neq K} n_j(\mathbf{y}_K) \times \int_{S_J} \mathrm{d}S_x\, \sigma^k_{ij}(\mathbf{x} - \mathbf{y}_K)\left[\frac{1}{S_J}F_{Jk} - \frac{5}{2}\eta_0\sum_m E_{km}n_m(\mathbf{x})\right] \quad (29)$$

This can be regarded as a lowest order correction for the variation in hydrodynamic stresses over the individual beads. The accuracy of this approximation shall be examined in subsection III.A in connection with the viscosity of a dimer of two identical beads. In eq 29, the first term on the right-hand side represents the "single sphere" contribution and the latter sum the correction due to the other beads. These correction terms fall off as r^{-2}. In principle, one could employ a more accurate approximation where eq 29 is used for the $\mathbf{f}$ terms appearing on the right-hand side of eq 27. This approach was not pursued in the present work since it would substantially complicate the mathematics.

For $J \neq K$, we expand $\mathbf{U}_{ij}(\mathbf{x} - \mathbf{x}_K)$ in eq 23 and $\sigma^k_{ij}(\mathbf{x} - \mathbf{y}_K)$ in eq 29 to second order about $\mathbf{x}_{JK} = \mathbf{x}_J - \mathbf{x}_K$.

Equation 23 becomes

$$-\frac{1}{2}\boldsymbol{E}\cdot(\mathbf{x}_K - \mathbf{d}) = \frac{1}{\zeta_K}\mathbf{F}_K + \sum_{J\neq K}\left\{\left[\frac{1}{\zeta_J}\boldsymbol{H}_{KJ} - \boldsymbol{B}_{KJ}\right]\cdot\mathbf{F}_J + \mathbf{b}_{KJ} - \mathbf{c}_{KJ} + \sum_{L\neq J}\{[\boldsymbol{C}_{KJL} + \boldsymbol{D}_{KJL} - \boldsymbol{G}_{KJL}]\cdot\mathbf{F}_L - \mathbf{d}_{KJL} + \mathbf{e}_{KJL}\}\right\} \quad (30)$$

$$\zeta_K = 6\pi\eta_0 a_K \quad (31a)$$

$$V_K = \frac{4}{3}\pi a_K^3 \quad (31b)$$

$$\boldsymbol{H}_{KJ} = \frac{3a_J}{4r}\left(\boldsymbol{I} + \frac{1}{r^2}\mathbf{rr}\right) - \frac{3a_J^3}{4r^3}\left(\frac{1}{r^2}\mathbf{rr} - \frac{1}{3}\boldsymbol{I}\right) \quad (31c)$$

$$\mathbf{r} = \mathbf{x}_{JK} \quad (31d)$$

$$\mathbf{r}' = \mathbf{x}_{LJ} \quad (31e)$$

$$(\boldsymbol{B}_{KJ})_{im} = \frac{3V_K}{20\zeta_K}\sum_j (\boldsymbol{\sigma}^m_{jl,j}(\mathbf{r}) + \boldsymbol{\sigma}^m_{jj,l}(\mathbf{r})) \quad (31f)$$

$$(\mathbf{b}_{KJ})_i = \frac{\pi\eta_0 a_J^3 V_K}{2\xi_K}\sum_{jmp}(\boldsymbol{\sigma}^m_{ij,pj}(\mathbf{r}) + \boldsymbol{\sigma}^m_{jj,pi}(\mathbf{r}))E_{pm} \quad (31g)$$

$$(C_{KJL})_{im} = V_J\sum_{jk} U_{ij,k}(\mathbf{r})\,\sigma^m_{jk}(\mathbf{r}') \quad (31h)$$

$$(\mathbf{c}_{KJ})_i = \frac{5}{2}\eta_0 V_J\sum_{jk} U_{ij,k}(\mathbf{r})E_{jk} \quad (31i)$$

$$(\boldsymbol{D}_{KJL})_{im} = V_J\left(\frac{a_L^2}{6} + \frac{b_J^2}{10}\right)\sum_{jk} U_{ij,k}(\mathbf{r})\,\nabla^2\sigma^m_{jk}(\mathbf{r}') \quad (31j)$$

$$(\mathbf{d}_{KJL})_i = \frac{10}{3}\pi\eta_0 a_L^3 V_J\sum_{jkmp} U_{ij,k}(\mathbf{r})\,\sigma^m_{jk,p}(\mathbf{r}')E_{mp} \quad (31k)$$

$$(\mathbf{e}_{KJL})_i = \frac{V_J}{3}\pi\eta_0 a_J^2 a_L^3\sum_{jkmpq} U_{ij,km}(\mathbf{r})[\sigma^q_{jk,mp}(\mathbf{r}') + \sigma^q_{jm,kp}(\mathbf{r}')]E_{qp} \quad (31l)$$

$$(\boldsymbol{G}_{KJL})_{im} = \frac{V_J}{10}a_J^2\sum_{jkp} U_{ij,kp}(\mathbf{r})[\sigma^m_{jk,p}(\mathbf{r}') + \sigma^m_{jp,k}(\mathbf{r}')] \quad (31m)$$

$$U_{ij,k}(\mathbf{r}) = \frac{1}{8\pi\eta_0}[r^{-3}(r_i\delta_{jk} + r_j\delta_{ik} - r_k\delta_{ij}) - 3r^{-5}r_ir_jr_k] \quad (31n)$$

$$U_{ij,km}(\mathbf{r}) = \frac{1}{8\pi\eta_0}[r^{-3}(\delta_{im}\delta_{jk} + \delta_{jm}\delta_{ik} - \delta_{km}\delta_{ij}) - 3r^{-5}(r_ir_m\delta_{jk} + r_jr_m\delta_{ik} + r_jr_k\delta_{im} + r_ir_k\delta_{jm} + r_ir_j\delta_{km} - r_kr_m\delta_{ij}) + 15r^{-7}r_ir_jr_kr_m] \quad (31o)$$

$$\sigma^k_{ij,m}(\mathbf{r}) = -\frac{3}{4\pi}[r^{-5}(r_ir_j\delta_{km} + r_ir_k\delta_{jm} + r_jr_k\delta_{im}) - 5r^{-7}r_ir_jr_kr_m] \quad (31p)$$

$$\sigma^k_{ij,mp}(\mathbf{r}) = -\frac{3}{4\pi}[r^{-5}(r_i\delta_{jp}\delta_{km} + r_j\delta_{ip}\delta_{km} + r_i\delta_{kp}\delta_{jm} + r_k\delta_{ip}\delta_{jm} + r_j\delta_{kp}\delta_{im} + r_k\delta_{jp}\delta_{im}) - 5r^{-7}(r_ir_jr_p\delta_{km} + r_ir_kr_p\delta_{jm} + r_jr_kr_p\delta_{im} + r_ir_jr_k\delta_{pm} + r_ir_jr_m\delta_{pk} + r_ir_kr_m\delta_{pj} + r_jr_kr_m\delta_{ip}) + 35r^{-9}r_ir_jr_kr_mr_p] \quad (31q)$$

Equation 30 is used to calculate the bead force, $\mathbf{F}_K$, for $K = 1$ to N. It can be written in compact form

$$\mathbf{a}_K = \mathbf{a}^0_K - \sum_{J\neq K}\sum_{L\neq J}\boldsymbol{P}_{KJL}\cdot\mathbf{F}_L = \sum_J \boldsymbol{Q}_{KJ}\cdot\mathbf{F}_J \quad (32)$$

where

$$\mathbf{a}^0_K = -\frac{1}{2}\boldsymbol{E}\cdot(\mathbf{x}_K - \mathbf{d}) + \sum_{J\neq K}(-\mathbf{b}_{KJ} + \mathbf{c}_{KJ} + \sum_{L\neq J}(\mathbf{d}_{KJL} - \mathbf{e}_{KJL})) \quad (33)$$

$$\boldsymbol{P}_{KJL} = \boldsymbol{C}_{KJL} + \boldsymbol{D}_{KJL} - \boldsymbol{G}_{KJL} \quad (34)$$

$$\boldsymbol{Q}_{KJ} = \frac{1}{\zeta_K}\boldsymbol{I}\delta_{JK} + (1 - \delta_{JK})\left[\frac{1}{\zeta_J}\boldsymbol{H}_{KJ} - \boldsymbol{B}_{KJ}\right] \quad (35)$$

Once a structure is defined, all of the terms appearing in eqs 30−35 can be computed except for the **F**'s. The difficulty with eq 32 is that the forces appear on both sides of the equation. In order to deal with this difficulty, we adapt an iterative approach in which approximate $\mathbf{F}_L$'s are used on the left-hand side of eq 32. In the first iteration, we simply set the $\mathbf{F}_L$'s to zero and then $\mathbf{a}_K$ is known for each of the N subunits of the bead array. Now define the $3N \times 1$ column vector, **A**, as consisting of the $3N \times 1$ column vectors, $\mathbf{a}_K$, stacked on top of each other. The $3N \times 1$ column vector, **F**, is defined in a similar way. Also, introduce the $3N \times 3N$ matrix, **Q**:

$$\boldsymbol{Q} = \begin{pmatrix} \boldsymbol{Q}_{11} & \cdots & \boldsymbol{Q}_{1N} \\ \vdots & \ddots & \vdots \\ \boldsymbol{Q}_{N1} & \cdots & \boldsymbol{Q}_{NN} \end{pmatrix} \quad (36)$$

This matrix can be inverted to yield $\mathbf{Q}^{-1}$. Then eq 32 can be written

$$\mathbf{F} = \boldsymbol{Q}^{-1}\cdot\mathbf{A} \quad (37)$$

This will yield the first estimated forces. These forces can then be used to recompute $\mathbf{a}_K$. Equation 37 is then used to obtain revised forces. This procedure is repeated until the forces converge. Our experience has been that, for a touching bead array, about 10 iterations are needed to obtain well-converged forces.

II.C. Viscosity Shape Factor. For a particular model structure, it is necessary to compute the forces on the bead array in five different elementary shear fields.[36] These elementary shear fields can be written

$$\boldsymbol{E}^{(1)} = \gamma(\boldsymbol{e}_1\boldsymbol{e}_2 + \boldsymbol{e}_2\boldsymbol{e}_1) \quad (38a)$$

$$\boldsymbol{E}^{(2)} = \gamma(\boldsymbol{e}_1\boldsymbol{e}_3 + \boldsymbol{e}_3\boldsymbol{e}_1) \quad (38b)$$

$$\boldsymbol{E}^{(3)} = \gamma(\boldsymbol{e}_2\boldsymbol{e}_3 + \boldsymbol{e}_3\boldsymbol{e}_2) \quad (38c)$$

$$\boldsymbol{E}^{(4)} = \gamma(\boldsymbol{e}_1\boldsymbol{e}_1 - \boldsymbol{e}_2\boldsymbol{e}_2) \quad (38d)$$

$$\boldsymbol{E}^{(5)} = \gamma(\boldsymbol{e}_1\boldsymbol{e}_1 - \boldsymbol{e}_3\boldsymbol{e}_3) \quad (38e)$$

$\mathbf{e}_a$ is a unit vector in direction a, and γ is the shear gradient (units of 1/s).

For each of the five elementary shear fields, the forces are computed as discussed previously. Then elementary shape factors are computed for each shear field,[36] and the result is

$$\xi_{ij}^{(t)} = -\frac{1}{2\eta_0\gamma V_T}\sum_{K=1}^{N}[\sum_{J\neq K}((\mathbf{x}_{Ki} - \mathbf{d}_i)\mathbf{F}_{Kj}^{(t)} + (\mathbf{x}_{Kj} - \mathbf{d}_j)\mathbf{F}_{Ki}^{(t)}] + \frac{5}{4\gamma}(E_{ji}^{(t)} + E_{ij}^{(t)}) + \sum_{K=1}^{N}\sum_{J\neq K=1}^{N}\left\{-\frac{V_K}{2\eta_0\gamma V_T}\times \sum_m(\sigma_{ij}^m + \sigma_{ji}^m)F_{Jm}^{(t)} + \frac{5\pi}{3\gamma V_T}V_K a_J^3\sum_{mp}(\sigma_{ji,p}^m + \sigma_{ij,p}^m)E_{mp}^{(t)} - \frac{V_K}{2\eta_0\gamma V_T}\left(\frac{a_J^2}{6} + \frac{b_K^2}{10}\right)\sum_m(\nabla^2\sigma_{ij}^m + \nabla^2\sigma_{ji}^m)F_{Jm}^{(t)}\right\} \quad (39)$$

In eq 39, V_T is the total volume of the bead array ($\sum_J V_J$), and the argument of the σ's appearing in eq 39 is $\mathbf{x}_{JK}$. Also

$$\nabla^2\sigma_{ij}^m = \sum_p \sigma_{ij,pp}^m \quad (40)$$

where the individual terms on the right-hand side of eq 40 are given by eq 31q.

Finally, the link between theory and experiment is the shape factor, ξ, which comes from an average over all orientations of the rigid model particles in all shear fields.[36] It is given by

$$\xi = \frac{1}{5}(\xi_{12}^{(1)} + \xi_{13}^{(2)} + \xi_{23}^{(3)}) + \frac{1}{15}(\xi_{11}^{(4)} + \xi_{33}^{(4)} - 2\xi_{22}^{(4)} + \xi_{11}^{(5)} + \xi_{22}^{(5)} - 2\xi_{33}^{(5)}) \quad (41)$$

III. Results

III.A. Dumbbell Dimer of Two Identical Beads. A dimer of two identical beads provides an excellent model system to test the equations derived in section II. Past studies of a touching dimer of two identical beads yield $\xi = 3.45$[38,39] or 3.58 (page 263 of ref 39). Recent "extrapolated shell" bead model calculations yield a value close to the lower value of 3.45.[21] Also, recent BE calculations using the BEST program[15] yield $\xi = 3.449$, which is in excellent agreement with ref 38 (Sergio Aragon, personal correspondence). In test cases of prolate and oblate ellipsoids, the BEST program yields ξ values that are accurate to better than 0.01%.[15] On that basis, it is safe to say with considerable confidence that the exact value of ξ for a touching dimer of two beads is 3.45. Shown in Figure 2 is a comparison of extrapolated shell (filled squares) and bead model results (eqs 39 and 41) for dimers composed of two identical beads or radius a and interbead separation R. The worst agreement is seen for touching beads, where the bead model shape factor falls below the exact value by 5.2%. For R/a between 3 and 4, the discrepancy is less than 2%. For the sake of comparison, the extended Kirkwood−Riseman shape factor, ξ, for a touching bead model reportedly exceeds the extrapolated shell model value (from a bead model calculation) by 19% (see Table 2 of ref 2 and also ref 21). Although eqs 39 and 41 yield *approximate* viscosities, they represent a significant improvement over past studies employing the same number of subunits.

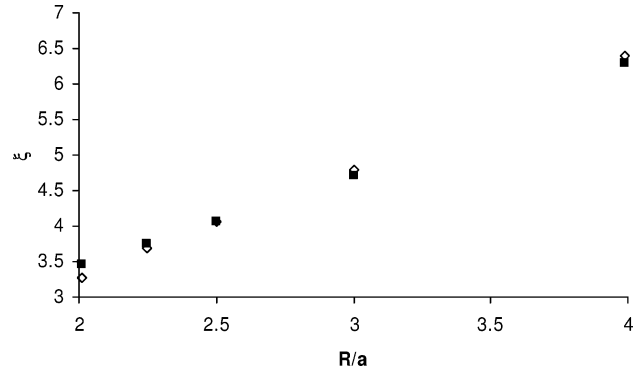

Figure 2. ξ versus R/a for dimers of two identical beads. R is the center-to-center distance between the two beads, and a is the bead radius. Filled squares come from BE extrapolated shell calculations, and unfilled diamonds come from the bead methodology developed in this work (eqs 39 and 41).

III.B. Rigid Rods and Simple Bead Arrays. We shall next consider linear strings of N identical touching beads of radius a. They shall be compared to viscosity shape factors of right circular cylinders of length L and axial radius R where BE results are available.[14] Intrinsic viscosities/shape factors of cylinders modeled as shells of beads have also been reported.[40] Structurally, bead and cylinder models are different from each other and this makes a direct comparison impossible. Nonethelss, bead and cylinder (or wormlike chain) models have been used interchangeably to describe duplex DNA with considerable success.[41−44] We start by setting the volumes of bead and right circular cylinder models equal:

$$\pi R^2 L = \frac{4}{3}\pi a^3 N \quad (42)$$

Introduce a dimensionless length variable, λ, by the definition

$$L = 2a(N - \lambda) \quad (43)$$

On physical grounds, we expect $0 < \lambda < 1$. An optimal value for this parameter shall be determined by finding that number between 0 and 1 that gives the best agreement for viscosity shape factors for bead models using eqs 39 and 41 and BE calculations on right circular cylinders. For the moment, however, λ shall be left as an adjustable parameter. Using eq 43 in eq 42

$$a = \sqrt{\frac{3}{2}}R\left(1 - \frac{\lambda}{N}\right)^{1/2} \quad (44)$$

Provided $\lambda/N \ll 1$, $a \cong (3/2)^{1/2}R$. For $R = 1.0$ nm, which is appropriate for duplex DNA,[45,46] $a \cong 1.225$ nm. This is the appropriate bead radius for large N. For small N, eq 44 can be used once λ is known. Also define the dimensionless variable

$$p = \frac{L}{2R} = \sqrt{\frac{3}{2}}N\left(1 - \frac{\lambda}{N}\right)^{3/2} \quad (45)$$

Figure 3 displays shape factors for right circular cylinders (filled squares) and bead models (unfilled diamonds) versus p. A value of $\lambda = 0.45$ yields the best agreement between the two models. The solid line represents a quadratic fit to the data ($1.5 < p < 18$) which can be written

$$\xi = 1.912 + 0.702p + 0.0495p^2 \quad (46)$$

The viscosity of a bead array is fairly sensitive to how the beads are arranged in space, or the conformation of the bead array. This is illustrated in Figure 4 for different conformations of tetramers modeled as four identical beads. In addition to the models, the viscosity shape factors are also given in the figure caption. The most compact structure, the ring of four beads, has the smallest ξ, and the most extended, the straight rod, has the largest. In this example, $\xi_{rod}/\xi_{ring} = 1.58$, and this, in turn, demonstrates the sensitivity of viscosity to particle conformation in general.

III.C. Comparison with Experiment: Amino Acids and Simple Peptides. Systems involving few subunits where the present work would be useful include cross-linked macromolecules,[47] duplex DNA,[48,49] and peptides.[50]

To date, there appears to be very little data available with regard to the viscosities of peptides, but there have been a number of investigations of the viscosity of dilute amino acids in aqueous solution. Before discussing the viscosity of amino acids, it will prove convenient to provide some background information on experimental viscosity measurements. There are three common conventions of reporting viscosities of dilute suspensions of weight concentration, c' (typically in g/dm^3), or number concentration, c (typically in mol/dm^3). Also let η denote the viscosity of the suspension, η_0 is the solvent viscosity, and V_p is the particle volume (typically in dm^3/mol). The first convention is the dimensionless viscosity "shape factor", ξ, introduced in subsection II.C:

$$\xi = \lim_{c\to 0} \frac{1}{cV_p}\left(\frac{\eta}{\eta_0} - 1\right) \quad (47)$$

Equation 47 provides the important link between theory and experiment. It should be remembered that the particle is being modeled, in the present work, as a bead array where fluid and particle velocities match on the surfaces enclosing V_p. (See eq 7.) Phyiscally, V_p includes both the "dry" volume of the particle and any solvent that moves with the particle as a rigid body. Thus, V_p could include a hydration layer of solvent.[20] The second convention is the intrinsic viscosity, $[\eta]$ (typically in dm^3/g)

$$[\eta] = \lim_{c'\to 0} \frac{1}{c'}\left(\frac{\eta}{\eta_0} - 1\right) \quad (48)$$

The third convention is the viscosity "B-factor" (typically in dm^3/mol) defined by

$$B = \lim_{c\to 0} \frac{1}{c}\left(\frac{\eta}{\eta_0} - 1\right) \quad (49)$$

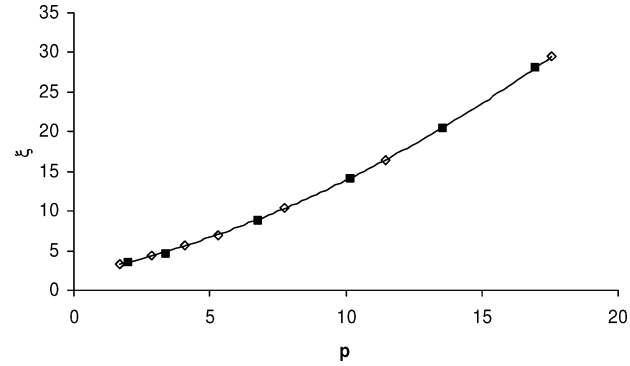

Figure 3. ξ versus p for straight rod models. See eq 46 for a definition of p. Also, $\lambda = 0.45$ in eq 46. Filled squares correspond to BE model studies of right circular cylinders.[14] Unfilled diamonds correspond to the bead methodology using eqs 39 and 41.

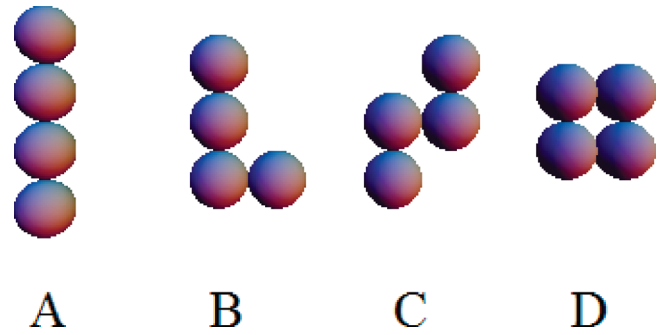

Figure 4. Tetramers of four identical beads. For structures A, B, C, and D, $\xi = 5.57$, 4.70, 4.17, and 3.53, respectively.

TABLE 1: B-Factors, Partial Molar Volumes, V_2, and Approximate Shape Factors, ξ^*

species	B (dm^3/mol)	V_2 (dm^3/mol)	ξ^*
Ala	0.251	0.0604	4.16
Gly	0.143	0.0432	3.31
Leu	0.576	0.1077	5.35
Phe	0.599	0.1236	4.85
Pro	0.279	0.0829	3.36
Ser	0.225	0.0607	3.71
Thr	0.335	0.0769	4.36
Val	0.423	0.0907	4.66
Gly-Gly	0.352	0.0763	4.61

Let M be the particle molecular weight (typically in g/mol). Then the three quantities are related to each other by

$$B = V_p\xi = M[\eta] \quad (50)$$

B-factors and also partial molar aqueous volumes in the limit of infinite dilution, V_2, of several amino acids as well as diglycine have been reported.[51−54] Experimental values are summarized in Table 1. B-factors for Gly, Ala, Leu, Val, and Gly-Gly come from ref 52, and the corresponding V_2 values come from ref 54. B and V_2 for Phe come from ref 53, whereas B and V_2 for Ser, Thr, and Pro come from ref 51. The B-factors appear to be reproducible to within a relative error of about 5%. Also shown in Table 1 are approximate shape factors, ξ^*, defined by

$$\xi^* = \frac{B}{V_2} \quad (51)$$

By comparing eqs 51 and 50, it is seen that ξ^* equals ξ if we set $V_2 = V_p$. The V_2 values were estimated from dilute aqueous solution density measurements.[51,53,54] Since V_p reflects the particle volume (per mole) within the surface of hydrodynamic shear, and V_2 corresponds to the excluded volume of the solvated particle, they may not, in fact, be equal. For the moment, however, we shall simply assume that $V_2 = V_p$.

Note that all of the ξ^* values in Table 1 exceed the value of 2.5 appropriate for a sphere with stick hydrodynamic boundary conditions. The most straightforward explanation for this is that the species are nonspherical and that shape is responsible for the departure of ξ^* from 2.5. On the basis of our earlier analysis of dimers and simple bead arrays, the approximate shape factors for Gly, Pro, and Ser of 3.3−3.7 are well explained in terms of a touching dimer model of two equivalent beads. To carry this argument further, next consider diglycine (Gly-Gly) and model it as a tetramer of four beads. Basically, diglycine is formed when two glycines dimerize and lose water. Figure 4 gives a range of possible conformations, and the ξ^* value of 4.61 from Table 1 is compatible with structure B in the figure. For the remaining amino acids (Ala, Leu, Phe, Thr, and Val) appearing in Table 1, model structures more complex than dimers are necessary to account for the ξ^* values observed. As Figure 4 demonstrates, however, even simple tetramer models are able to account for the range in ξ^* values observed. For more realistic surface models that account *in detail* for the actual solvent accessible surface of the amino acid or dipeptide, bead[10,20] or BE[15] methodologies woud be more appropriate than the methodology developed in the present work. What the present analysis shows is that the intrinsic viscosities of amino acids and simple peptides can be explained reasonably well by nonspherical particles of an overall size compatible with their known partial molar volumes.

We would like to carry the analysis of the viscosity of the amino acids (and Gly-Gly) further in a way that avoids setting $V_p = V_2$ as done in the previous paragraph. A more appropriate molecular volume would come from transport measurements of which viscosity is one example. Translational diffusion constants, D_T, of the amino acids in the limit of low concentration have been reported by a number of investigators.[55−59] The diffusive or "hydrodynamic" radius, R_D, shall be defined

$$R_D = \frac{k_B T}{6\pi\eta_0 D_T} \tag{52}$$

where k_B is Boltzmann's constant and T is absolute temperature. The physical significance of R_D is that it corresponds to the radius of a suspension of dilute spheres that diffuse at the same rate as the particles in the actual suspension. It should be emphasized that we are not assuming our actual suspension is made up of spherical particles. Also introduce the "stick" diffusion constant of a sphere of volume V_p/N_{Av} (N_{Av} is Avogadro's number), D_0, where V_p is the actual molar particle volume as defined following eq 47.

$$D_0 = \frac{k_B T}{6\pi\eta}\left(\frac{4\pi N_{Av}}{3V_p}\right)^{1/3} \tag{53}$$

Also define the reduced translational diffusion constant, X.

$$X = \frac{D_T}{D_0} \tag{54}$$

For nonspherical particles, X will deviate from 1.

In analogy to the diffusive radius, we can define the viscous radius, R_η, which corresponds to the radius of a dilute suspension of spheres that gives the same B as the actual suspension. Setting $\xi = 2.5$ and $V_p = 4\pi N_{Av} R_\eta^3/3$ (appropriate for spheres) in eq 50

$$R_\eta = \left(\frac{3B}{10\pi N_{Av}}\right)^{1/3} \tag{55}$$

We can now use eqs 50 and [52−55] to eliminate V_p:

$$\frac{R_\eta}{R_D} = \left(\frac{2\xi}{5}\right)^{1/3} X \tag{56}$$

Equation 56 is closely related to the Scheraga−Mandelkern parameter[60] and provides a way of eliminating V_p and isolating the shape dependence by combining the results from two independent transport measurements. This same ratio (called IT in ref 61) has been studied for a wide variety of macromolecules and bioparticles.[61] In the present case, these are viscosity and translational diffusion, and in ref 60, it was viscosity and sedimentation. An alternative, but closely related, approach involves viscosity and rotational diffusion relaxation times.[2,62] An advantage of the Harding approach of refs 2 and 62 is its greater sensitivity to particle shape, but this approach requires rotational relaxation times that are not available to us.

Summarized in Table 2 are R_η, R_D, and R_η/R_D for the same species given in Table 1. For the diffusive radii listed, values for Leu and Pro come from ref 55; the value for Phe comes from ref 57; values for Ala, Thr, and Val come from ref 58, and the value for Ser comes from ref 59. Values for Gly and Gly-Gly have also been available for many years,[56] but for the present work, we use results from recent field gradient NMR measurements (H. Pei, M. W. Germann, S. A. Allison, manuscript in preparation). It should be emphasized that R_η and R_D in Table 2 have been extracted from experiment and no assumptions beyond the operational definitions of R_η and R_D have been used. We shall next consider what modeling predicts for R_η/R_D for some simple structures. For prolate and oblate ellipsoids, right circular cylinders, and toroids, results from ref 14 are used. For the tetramer bead arrays, eqs 39 and 40 are used for ξ. For X, we employ a closely related procedure for the translation of bead arrays that accounts for the variation in hydrodynamic stresses over the bead surfaces.[63] For the touching dimer, exact values are used.[21,38,64] The results are summarized in Table 3.

For compact structures listed in Table 3, R_η/R_D lies close to 1.01 and lower. Even for needlelike structures such as the $a/b = 10$ prolate ellipsoid and the $p = 17$ rod, R_η/R_D lies in the range 1.14−1.21. From Table 2, on the other hand, R_η/R_D ranges from 1.14 (for Gly) to 1.345 (for Phe). Even for Gly, this corresponds to a highly nonspherical particle and this seems unrealistic on structural grounds. One possible explanation for the anomalously large R_η/R_D values seen in Table 2 is related to the validity of continuum stick hydrodynamic boundary conditions in adequately describing the solvent−particle interface for a particle/molecule as small as an amino acid in an aqueous solvent. Studies on the rotational reorientation time of

TABLE 2: Viscous and Diffusive Radii

species	R_η (nm)	R_D (nm)	R_η/R_D
Ala	0.341	0.267	1.28
Gly	0.283	0.248	1.14
Leu	0.450	0.339	1.33
Phe	0.456	0.347	1.34
Pro	0.354	0.268	1.32
Ser	0.329	0.276	1.19
Thr	0.376	0.304	1.24
Val	0.406	0.332	1.22
Gly-Gly	0.382	0.324	1.19

TABLE 3: X, ξ, and R_η/R_D for Some Simple Structures

structure	details[a]	X	ξ	R_η/R_D[b]
oblate ellipsoid	$a/b = 10$	0.689	7.92	1.012
oblate ellipsoid	$a/b = 2$	0.962	2.84	1.004
sphere	($a/b = 1$)	1.00	2.50	1.000
sphere[c]	($a/b = 1$)	1.50	1.00	1.105
prolate ellipsoid	$a/b = 2$	0.958	2.91	1.008
prolate ellipsoid	$a/b = 5$	0.801	5.78	1.059
prolate ellipsoid	$a/b = 10$	0.650	13.52	1.141
prolate ellipsoid[c]	$a/b = 10$	5.48	7.06	7.74
cylinder	$p = 2.04$	0.904	3.43	1.004
cylinder	$p = 17.0$	0.543	28.0	1.214
toroid	$P = 2.0$	0.868	3.87	1.004
toroid	$p = 10.0$	0.494	24.0	1.050
dimer	identical touching beads	0.906	3.45	1.009
tetramer	D of Figure 4	0.898	3.53	1.007
tetramer	B of Figure 4	0.821	4.70	1.013
tetramer	A of Figure 4	0.797	5.57	1.041

[a] For ellipsoids, a/b is the major axis/minor axis; for rods, p is given by eq 46; for toroids, $p = R/r$, where R and r are the outer and inner toroidal radii.[14] [b] From eq 56. [c] Slip boundary conditions.

small molecules such as methyl acetate in water indicate that a hydrodynamic boundary condition intermediate between stick and "slip" is more appropriate.[65] In the case of slip boundary conditions, only the normal velocity component of fluid and particle match at the interface. In addition, however, there is no tangential component of normal stress at the interface.[14,66] In addition to the mostly "stick" models considered in Table 3, two "slip" models have also been included for a sphere and a prolate ellipsoid with $a/b = 10$. In these cases, X and ξ come from ref 14. Since $(R_\eta/R_D)_{slip} > (R_\eta/R_D)_{stick}$ for both geometries, particularly for the prolate ellipsoid, this interpretation is not unreasonable. Although moving to a model with boundary conditions intermediate between "stick" and "slip" may help reconcile theory and experiment for low molecular weight peptides in an aqueous solvent, it will not work for certain systems such as low molecular weight alkanes in benzene solvent.[67] In this system, the intrinsic viscosity of low molecular weight alkanes is actually negative. The work of Fixman[27] provides insight into how this problem could be dealt with from the standpoint of modeling.

IV. Summary

In modeling the viscosity of a dilute bead array at low shear, substantial error arises when account is not taken of the variation in hydrodynamic stress forces over individual beads. This problem can be addressed in two very different ways. In the first approach, one simply uses many beads or plates to model the particle surface. Over the past 15 years, a number of thorough studies have been carried out on the viscosities of proteins. Detailed models have been constructed from known crystal structures, and model intrinsic viscosities have been compared with experiment. This comparison can provide valuable information about solution conformation and hydration. Both bead[2,10,11,20] and BE[13,15] procedures have been used with considerable success. Typically, 1000−3000 beads[10] or 2000−4000 plates[15] have been employed in these studies. In an alternative approach followed in the present work, the number of beads is kept comparatively small, but approximate account is taken of the variation in hydrodynamic stresses over the individual bead surfaces. For a dimer of two touching identical beads, the methodology developed here is off by 5.2%. One area where the present methodology is expected to be useful is for flexible structures where many conformations have to be sampled. This includes cross-linked macromolecules,[47] duplex DNA,[48,49] and peptides.[50] In the present study, we have shown how a bead model in viscosity modeling can be used as a substitute for a right circular cylinder. In future work, we hope to extend this to a flexible worklike chain[41−44] which is an excellent model for duplex DNA.

We ended the Results section of this paper with an analysis of viscosity and translational diffusion data of amino acids and diglycine. These are small molecules not much larger than the solvent which is being modeled as a hydrodynamic continuum. We conclude that a model in which stick hydrodynamic boundary conditions are assumed is unable to account for the observed viscosity/diffusion data. Consistent with earlier studies[65] on molecules of a comparable size in aqueous solvent, hydrodynamic boundary conditions intermediate between stick and slip appear to be appropriate. This is a problem that warrants further theoretical study such as detailed BE modeling using different hydrodynamic boundary conditions.[14−16] For fairly large macromolecules such as proteins, nucleic acids, and other bioparticles, stick boundary conditions appear to give model intrinsic viscosities in agreement with experiment.[15,20,21] Anomalous intrinsic viscosities appear to be restricted to solutes that are small or comparable in size to the solvent. In certain systems such as low molecular weight alkanes in benzene where the intrinsic viscosity is negative,[67] it may be possible to deal with this by including direct forces ($\mathbf{s} \neq 0$) in modeling.[27] This is a problem for future study.

Acknowledgment. We would like to thank Prof. Sergio Aragon of San Francisco State University for providing us with accurate BE calculations for the transport properties of two identical touching spheres.

References and Notes

(1) Cantor, C. R.; Schimmel, P. R. *Biophysical Chemistry, Part II: Techniques for the Study of Biological Structure and Function*; 1980; Chapter 12.
(2) Harding, S. E. *Prog. Biophys. Mol. Biol.* **1997**, *68*, 207.
(3) Einstein, A. *Ann. Phys.* **1911**, *34*, 591.
(4) Simha, R. *J. Phys. Chem.* **1940**, *44*, 25.
(5) Kirkwood, J. G.; Riseman, J. *J. Chem. Phys.* **1948**, *16*, 565.
(6) Debye, P.; Bueche, A. M. *J. Chem. Phys.* **1948**, *16*, 573.
(7) Garcia de la Torre, J.; Bloomfield, V. A. *Biopolymers* **1978**, *17*, 1605.
(8) Garcia Bernal, J. M.; Garcia de la Torre, J. *Biopolymers* **1980**, *19*, 751.
(9) Byron, O. *Biophys. J.* **1997**, *72*, 408.
(10) Garcia de la Torre, J.; Huertas, M. L.; Carrasco, B. *Biophys. J.* **2000**, *78*, 719.
(11) Byron, O. *Methods Enzymol.* **2000**, *321*, 278.
(12) Youngren, G. K.; Acrivos, A. *J. Fluid Mech.* **1975**, *65*, 377.
(13) Zhou, H.-X. *Biophys. J.* **1995**, *65*, 2286–2298.
(14) Allison, S. A. *Macromolecules* **1999**, *32*, 5304.
(15) Hahn, D. K.; Aragon, S. *J. Chem. Theory Comput.* **2006**, *2*, 1416.
(16) Aragon, S. *J. Comput. Chem.* **2004**, *25*, 1191.
(17) Zipper, P.; Durschlag, H. *Prog. Colloid Polym. Sci.* **1997**, *107*, 58.
(18) Zipper, P.; Durschlag, H. *Biochem. Soc. Trans.* **1998**, *26*, 726.
(19) Carrasco, B.; Garcia de la Torre, J.; Zipper, P. *Eur. Biophys. J.* **1999**, *28*, 510.

(20) Garcia de la Torre, J. *Biophys. Chem.* **2001**, *93*, 159.
(21) Garcia de la Torre, J.; del Rio Echenique, G.; Ortega, A. *J. Phys. Chem. B* **2007**, *111*, 955.
(22) Bloomfield, V. A.; Filson, D. P. *J. Polym. Sci., Part C: Polym. Symp.* **1968**, *25*, 73.
(23) Wilson, R. W.; Bloomfield, V. A. *Biopolymers* **1979**, *18*, 1205.
(24) Garcia de la Torre, J.; Bloomfield, V. A. *Q. Rev. Biophys.* **1981**, *14*, 81.
(25) Garcia de la Torre, J.; Rodes, V. *J. Chem. Phys.* **1983**, *79*, 2454.
(26) Garcia de la Torre, J.; Carrasco, B. *Eur. Biophys. J.* **1998**, *27*, 549.
(27) Fixman, M. *J. Chem. Phys.* **1990**, *92*, 6858.
(28) Ladd, A. J. C. *J. Chem. Phys.* **1990**, *93*, 3484.
(29) Cichocki, B.; Felderhof, B. U.; Hinsen, K.; Wajnryb, E.; Blawzdziewicz, J. *J. Chem. Phys.* **1994**, 3780.
(30) Allison, S. A.; Pei, H.; Haynes, M.; Xin, Y.; Law, L.; Labrum, J.; Augustin, D. *J. Phys. Chem. B* **2008**, *112*, 5858.
(31) Happel, J.; Brenner, H. *Low Reynolds Number Hydrodynamics*; Martinus Nijhoff: The Hague, 1983.
(32) Kim, S.; Karilla, S. J. *Microhydrodynamics*; Butterworth-Heinemann: Boston, 1991.
(33) Booth, F. *Proc. R. Soc. London, Ser. A* **1950**, *203*, 533.
(34) Sherwood, J. D. *J. Fluid Mech.* **1980**, *101*, 609.
(35) Watterson, I. G.; White, L. R. *J. Chem. Soc., Faraday Trans. 2* **1981**, *77*, 4464.
(36) Allison, S. A. *Macromolecules* **1998**, *31*, 4464.
(37) Landau, L. D.; Lifshitz, E. M. *Fluid Mechanics*; Pergamon Press: Oxford, U.K., 1959.
(38) Wakiya, S. *J. Phys. Soc. Jpn.* **1971**, *31*, 1581. Wakiya, S. *J. Phys. Soc. Jpn.* **1972**, *33*, 278.
(39) Brenner, H. *Int. J. Multiphase Flow* **1974**, *1*, 195.
(40) Ortega, A.; Garcia de la Torre, J. *J. Chem. Phys.* **2003**, *119*, 9914.
(41) Hagerman, P. J.; Zimm, B. H. *Biopolymers* **1981**, *20*, 1481.
(42) Hagerman, P. J. *Biopolymers* **1981**, *20*, 1503.
(43) Allison, S. A. *Macromolecules* **1986**, *19*, 118.
(44) Allison, S. A.; Schurr, J. M. *Macromolecules* **1997**, *30*, 7132.
(45) Eimer, W.; Williamson, J. R.; Boxer, S. G.; Pecora, R. *Biochemistry* **1990**, *29*, 799.
(46) Diaz, R.; Fujimoto, B. S.; Schurr, J. M. *Biophys. J.* **1997**, *72*, A322.
(47) Potschke, H.; Barnikol, W.; Kirste, R.; Rosenbaum, M. *Macromol. Chem. Phys.* **1996**, *197*, 1419.
(48) Eigner, J.; Doty, P. *J. Mol. Biol.* **1965**, *12*, 549.
(49) Harrington, R. E. *Biopolymers* **1980**, *19*, 449.
(50) Pei, H.; Xin, Y.; Allison, S. A. *J. Sep. Sci.* **2008**, *31*, 555.
(51) Ogawa, T.; Mizutani, K.; Yasuda, M. *Bull. Chem. Soc. Jpn.* **1984**, *57*, 2064.
(52) Banipal, T. S.; Singh, G. *Thermochim. Acta* **2004**, *412*, 63.
(53) Banipal, T. S.; Kauer, D.; Banipal, P. K. *J. Chem. Thermodyn.* **2006**, *38*, 1214.
(54) Banipal, T. S.; Singh, G. *J. Solution Chem.* **2003**, *32*, 997.
(55) Polson, A. *Biochem. J.* **1937**, *31*, 1903.
(56) Longsworth, L. G. *Electrochemistry in Biology and Medicine*; Shedlovsky, T., Ed.; Wiley: New York, 1955; Chapter 12.
(57) Cremasco, M. A.; Hritzko, B. J.; Xie, Y.; Wang, N. H. L. *Braz. J. Chem. Eng.* **2001**, *18*, 181.
(58) Ma, Y.; Zhu, C.; Ma, P.; Yu, K. T. *J. Chem. Eng. Data* **2005**, *50*, 1192.
(59) Germann, M. W.; Turner, T.; Allison, S. A. *J. Phys. Chem. A* **2007**, *111*, 1452.
(60) Scheraga, H. A.; Mandelkern, L. *J. Am. Chem. Soc.* **1953**, *75*, 179.
(61) Ortega, A.; Garcia de la Torre, J. *J. Chem. Phys.* **2007**, *8*, 2464.
(62) Harding, S. E. *Biochem. J.* **1980**, *189*, 359.
(63) Allison, S. A.; Pei, H.; Haynes, M.; Xin, Y.; Law, L.; Labrum, J.; Augustin, D. *J. Phys. Chem. B* **2008**, *112*, 5858.
(64) Swanson, E.; de Haen, C.; Teller, D. C. *J. Chem. Phys.* **1980**, *72*, 1623.
(65) Bauer, D. R.; Brauman, J. I.; Pecora, R. *J. Am. Chem. Soc.* **1974**, *96*, 6840.
(66) Hu, C.-M.; Zwanzig, R. *J. Chem. Phys.* **1974**, *60*, 4354.
(67) Dewan, K. K.; Bloomfield, V. A.; Berget, P. G. *J. Phys. Chem.* **1974**, *75*, 3120.

JP9001109